Nanoscale

PAPER

View Article Online
View Journal | View Issue

Cite this: *Nanoscale*, 2023, **15**, 10820

Cascade energy transfer boosted near-infrared circularly polarized luminescence of nanofibers from an exclusively achiral system†

Chen Xiao,[a,b] Chengxi Li,[b,c] Kang Huang,[b,c] Pengfei Duan *[b,c] and Yafei Wang *[a]

Received 1st April 2023,
Accepted 24th May 2023

DOI: 10.1039/d3nr01515g

rsc.li/nanoscale

We constructed chiral supramolecular nanofibers for light harvesting based on symmetry-breaking, and these can generate near-infrared circularly polarized luminescence (CPL) with high dissymmetry factor (g_{lum}) through a synergistic energy transfer and chirality transfer process. Firstly, the achiral molecule BTABA was assembled into a symmetry-breaking assembly using a seeded vortex strategy. Subsequently, the chiral assembly can endow the two achiral acceptors, Nile Red (NR) and Cyanine 7 (CY7), with supramolecular chirality, as well as chiroptical properties. CY7 can reach an excited state and emit near-infrared light through a cascade energy transfer process from BTABA to NR and then to CY7, but cannot directly acquire energy from the excited BTABA. Significantly, the near-infrared CPL of CY7 can be obtained with a boosted g_{lum} value of 0.03. This work will provide a deep insight into the preparation of materials with near-infrared CPL activity from an exclusively achiral system.

The wavelength range of near-infrared (NIR) light is defined as the region from 700 to 2500 nm,[1] which is widely used in the fields of biomedical imaging,[2] photodynamic therapy[3] and encryption.[4] If one focuses on the polarization dimension, near-infrared circularly polarized light can provide further information to effectively restrain interference, filtrate signals and enhance the signal–noise ratio. Generally speaking, circularly polarized luminescence (CPL) refers to the difference in the emission of the left-handed and right-handed circularly polarized light in chiral chromophores or chiral environments in the excited state. The luminescence dissymmetry factor is used to measure the quality of CPL, which can be defined as $g_{lum} = 2 \times (I_L - I_R)/(I_L + I_R)$, where I_L and I_R, respectively, refer to the intensity of left and right CPL.[5,6] Currently, there are few reports on the materials with near-infrared CPL activity.[7–9] Metal complexes modified with chiral ligands are generally used to generate CPL in the near-infrared region, but their g_{lum} values are relatively small.[10] A few lanthanide metal complexes show high near-infrared CPL activity and g_{lum}, but these molecules or their precursors are difficult to synthesize due to their complicated chiral structure.[11,12] Meanwhile, it is hard to flexibly adjust the Stokes-shift of near-infrared CPL.

Fortunately, chiral assembly and energy transfer strategies have been proven as important approaches for boosting CPL.[13–24] Based on this point, we considered using a supramolecular assembly as the chiral host to carry the fluorescent chromophores as the guests and achieve CPL with a tuneable Stokes shift in the near-infrared region through cascaded energy transfer among fluorescent chromophores. In addition, it has been demonstrated that symmetry-breaking is an effective way of constructing chiral supramolecular structures for achiral building blocks.[25–28] In our previous work, chirality-controlled supramolecular assemblies could be obtained through the seeded vortex method from exclusively achiral C_3-symmetric molecules.[29] More importantly, in the light-harvesting collection of the chiral assembly system, fluorescence resonance energy transfer (FRET) was expected to be an important process for further amplifying the g_{lum} value.[30,31]

For this purpose, we have used chiral assemblies made from achiral C_3-symmetric molecules to construct a cascade energy transfer system, which showed high g_{lum} values of near-infrared CPL. As shown in Fig. 1, we synthesized an achiral molecule (BTABA) and then prepared chiral assemblies through the seeded-vortex strategy. When BTABA molecules were co-assembled with Nile Red (NR) and Cyanine 7 (CY7),

[a]*National Experimental Demonstration Center for Materials Science and Engineering, Jiangsu Key Laboratory of Environmentally Friendly Polymeric Materials, Jiangsu Collaborative Innovation Center of Photovoltaic Science and Engineering, Jiangsu Engineering Laboratory of Light-Electricity-Heat Energy-Converting Materials and Applications, School of Materials Science & Engineering, Changzhou University, Changzhou, 213164, P. R. China.*
E-mail: wangyafei@cczu.edu.cn
[b]*CAS Key Laboratory of Nanosystem and Hierarchical Fabrication, National Center for Nanoscience and Technology (NCNST), No. 11 ZhongGuanCun BeiYiTiao, Beijing 100190, P. R. China. E-mail: duanpf@nanoctr.cn*
[c]*University of Chinese Academy of Sciences, Beijing 100049, P. R. China*
† Electronic supplementary information (ESI) available. See DOI: https://doi.org/10.1039/d3nr01515g

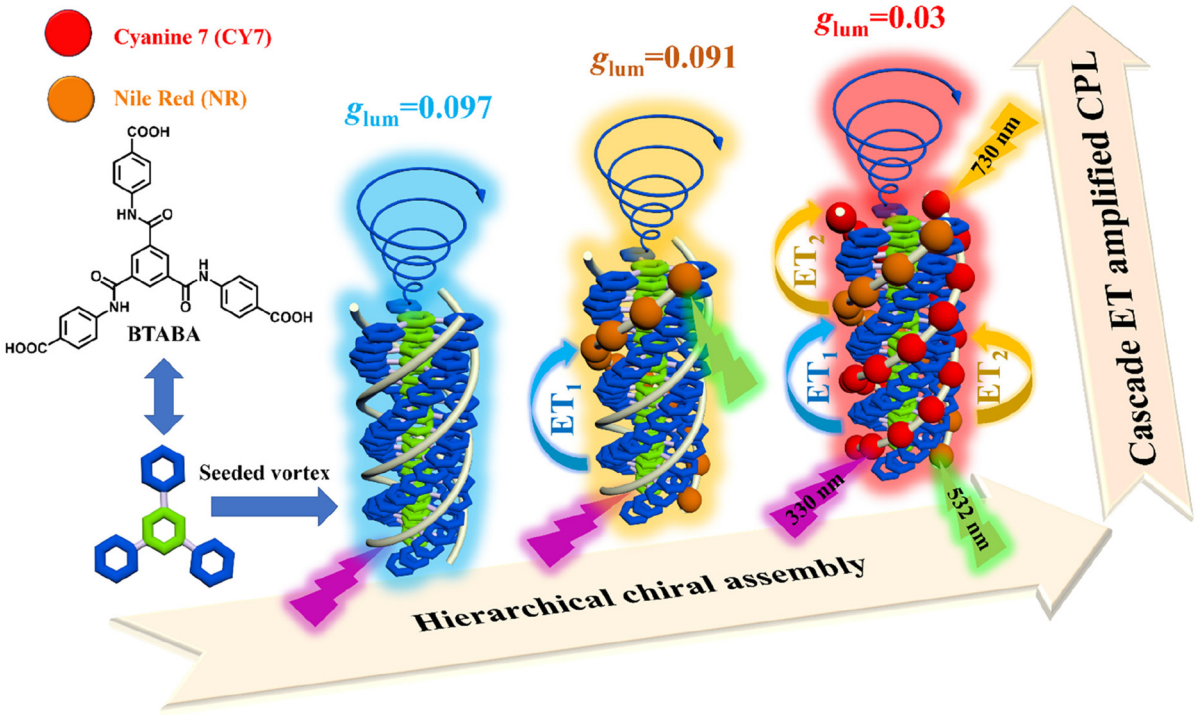

Fig. 1 A diagram illustrating the cascaded energy transfer in a non-chiral system. By employing a seed-induced vortex mixing strategy, chiral assemblies with controlled chirality were obtained. When Nile Red (NR) and Cyanine 7 (CY7) were co-assembled with BTABA, the chiral assemblies could transfer their chirality to non-chiral acceptors and achieve circularly polarized luminescence in the near-infrared region *via* cascaded energy transfer.

chiral assemblies of BTABA endowed the two achiral dyes with induced supramolecular chirality, where the g_{lum} values of energy acceptors were further amplified by the energy transfer from donors to acceptors. CY7 is responsible for the strong near-infrared CPL emission, which can be achieved by various excitation wavelengths according to the involvement of components in the system.

After seeded-vortex treatment, BTABA formed chiral supramolecular assemblies in a DMF/H_2O mixed solvent. As compared with the solution of BTABA, the absorption peak of the formed chiral assemblies was broadened, indicating the formation of π–π stacking during the self-assembly process of BTABA molecules.[32,33] The fluorescence intensity of the chiral assemblies was 15.7 times stronger than that of the solution state, accompanied by a pronounced red-shift from 368 nm to 448 nm (Fig. S1†). This might be due to the restriction of molecular internal rotation by aggregation, thereby reducing non-radiative transitions and resulting in fluorescence enhancement. Here, two achiral organic dyes, NR and CY7, were selected to co-assemble with BTABA. As shown in Fig. 2a and b, the absorption peak of NR overlaps with the emission peak of BTABA, indicating that NR is a suitable energy acceptor for BTABA. In addition, the emission maximum of NR is precisely located within the absorption range of CY7, enabling it to act as an energy mediator in the light-harvesting system.[34,35]

In BTABA assemblies, different amounts of NR were added. By increasing the NR ratio, it was observed that the emission peak at 465 nm decreased, and a new gradually increasing emission peak appeared at around 647 nm. This was attributed to the fluorescence emission of NR, indicating that NR can be regarded as an effective energy acceptor for BTABA (Fig. 2c). As shown in Fig. S2 and Table S1,† when the molar ratio of BTABA to NR was 60 : 1, the emission of NR reached the highest intensity, and the ET efficiency was approximately 80.5% by exciting BTABA. Further increasing the amount of NR will lead to aggregation-caused quenching (ACQ). Therefore, the ratio of BTABA : NR was chosen as 60 : 1, and CY7 as a second acceptor was further added. By exciting BTABA, the emission of the NR as the second energy donor showed decreasing emission intensity at 647 nm with increasing CY7 ratios, and a new fluorescence emission peak appeared at 805 nm, which belongs to the fluorescence emission of CY7 (Fig. 2e). When the molar ratio of BTABA/NR/CY7 was 60/1/1, the best emission of CY7 can be obtained without an obvious ACQ effect, and the ET efficiency was approximately 41.3%. This indicates that NR acts as a "bridge" towards the energy transfer from BTABA to CY7. It should be noted that in the BTABA/CY7 system, increasing CY7 will not influence the fluorescence intensity of BTABA and no CY7 emission occurs by exciting BTABA, indicating that energy transfer cannot occur between BTABA and CY7 (Fig. S3†). In order to further demonstrate the energy transfer process and reveal possible mechanisms, fluorescence lifetime measurements were conducted. As shown in Fig. 2d and f, the average lifetime of the

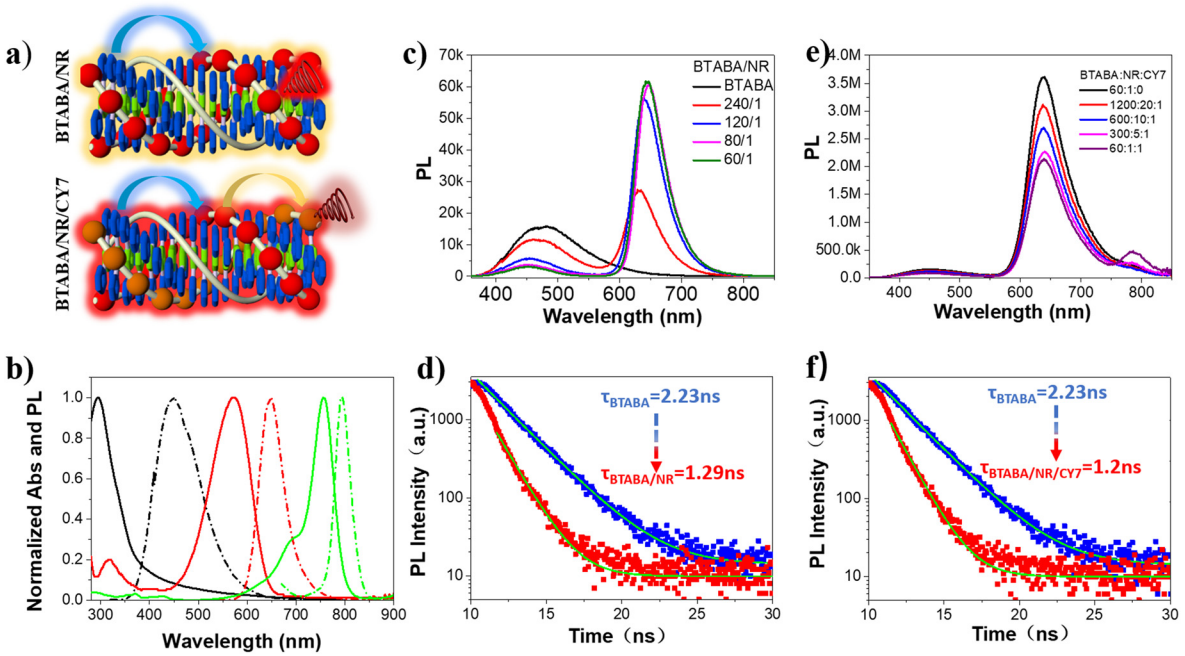

Fig. 2 (a) The diagram of energy transfer. (b) Normalized absorption (solid line) and emission (dashed line) spectra of the DMF solution of BTABA (black line), NR (red line) and CY7 (green line). (c) Fluorescence spectra of the BTABA/NR assembly in the presence of different amounts of NR. (d) Emission decay curves of the assembly of BTABA and BTABA/NR. (e) Fluorescence spectra of the BTABA/NR/CY7 assembly in the presence of different amounts of CY7. (f) Emission decay curves of the assembly of BTABA/NR and BTABA/NR/CY7. [BTABA] = 5.29 mM, [NR] = 0.088 mM, [CY7] = 0.088 mM.

donor BTABA in BTABA/NR and BTABA/NR/CY7 assemblies was shorter than that in the BTABA assembly, further demonstrating that the ET from the donor to the acceptor is efficient, and the energy transfer between BTABA and NR mainly follows the fluorescence resonance energy transfer mechanism,[36–38] while there is almost no change in the BTABA/CY7 assembly, further confirming that there is no efficient energy transfer between BTABA and CY7 (Fig. S4†). On the other hand, we tested the fluorescence lifetimes of pure NR and CY7 solutions, which were found to be 2.24 ns and 1.12 ns, respectively. The fluorescence lifetime of NR in the BTABA/NR assembly was 2.01 ns, indicating that the assembling process will not significantly change the lifetime of luminescence in dyes as compared to that in pure dye solutions (Fig. S4†). Overall, in this fluorescence resonance energy transfer system, we could obtain near-infrared emission at 805 nm by excitation at three wavelengths of 330 nm, 532 nm and 730 nm, and the longest Stokes shift can reach 470 nm.

We further investigated the chiral optical activity of the system. The completely achiral molecule BTABA exhibited strong supramolecular chirality during the vortex-assisted assembly process. As shown in Fig. S5,† the *M* and *P* assemblies of BTABA displayed strong and mirror-image circular dichroism (CD) signals. When the guest NR was co-assembled with BTABA, a new CD signal appeared at the absorption peak of the acceptor NR. In the BTABA/NR/CY7 assembly, CD signals of both achiral dyes could be observed simultaneously. In addition, the CD signal of CY7 could also be observed in the BTABA/CY7 assembly. It is worth noting that the chiral signals of both guests NR and CY7 have opposite CD signals to that of the chiral host of BTABA. These results indicate that the chiral host of the BTABA assembly can endow all guests with oppositely induced chirality.

At the same time, in the BTABA assembly system, due to the large number of functional groups that can provide hydrogen bonding and π–π interactions, non-covalent interactions can cause the BTABA molecules to orient themselves along the direction of the interaction forces and exhibit certain degrees of order on a macroscopic scale. In this case, the resulting anisotropy of the material further causes light scattering, which often accounts for a significant proportion of the CD signal so that the induced CD signal of the achiral dye is very weak and almost unobservable (Fig. S5†). Therefore, in this case, we further used fluorescence-detected circular dichroism (FDCD) to exclude the influence of material self-scattering on the induced chirality of the dyes.[39] As shown in the FDCD spectrum in Fig. 3c–e and S6,† a clear chiral signal appeared at 570 nm in the BTABA/NR assembly, which belongs to the characteristic chiral signal of NR. Correspondingly, both the achiral dye molecules NR and CY7 showed mirror-symmetric FDCD signals. Moreover, the FDCD signals of the achiral dye molecules were opposite to those of the chiral BTABA assemblies.

To further investigate the reasons why the chiral donor BTABA induced opposite-handedness in achiral dyes, we use DFT calculations to simulate the donor–acceptor structure. As

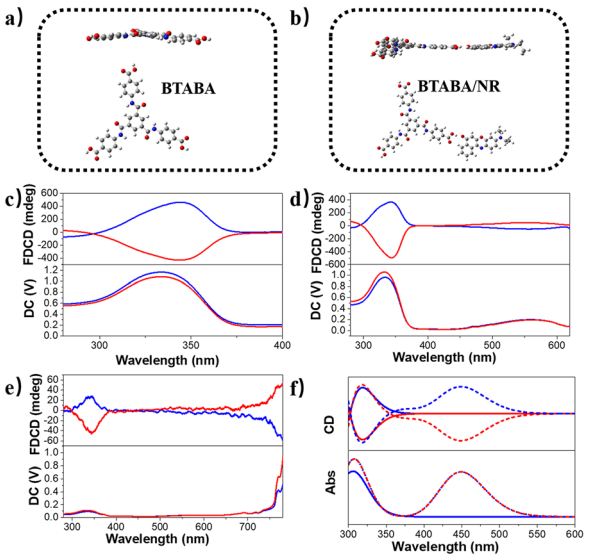

Fig. 3 The simulated chiral structure of (a) BTABA and (b) BTABA/NR. (c) FDCD spectra of *M*-BTABA (blue line) and *P*-BTABA (red line). The detected emission wavelength was set at 450 nm. (d) FDCD spectra of *M*-BTABA/NR (blue line) and *P*-BTABA/NR (red line). The detected emission wavelength was set at 640 nm. (e) FDCD spectra of *M*-BTABA/NR/CY7 (blue line) and *P*-BTABA/NR/CY7 (red line). The detected emission wavelength was set at 755 nm. (f) The CD simulation spectrum of BTABA (solid line) and BTABA/NR (dashed line), where CD spectra of *M*-BTABA and *P*-BTABA are indicated by the blue and red lines, respectively. [BTABA] = 5.29 mM, [NR] = 0.088 mM, [CY7] = 0.088 mM.

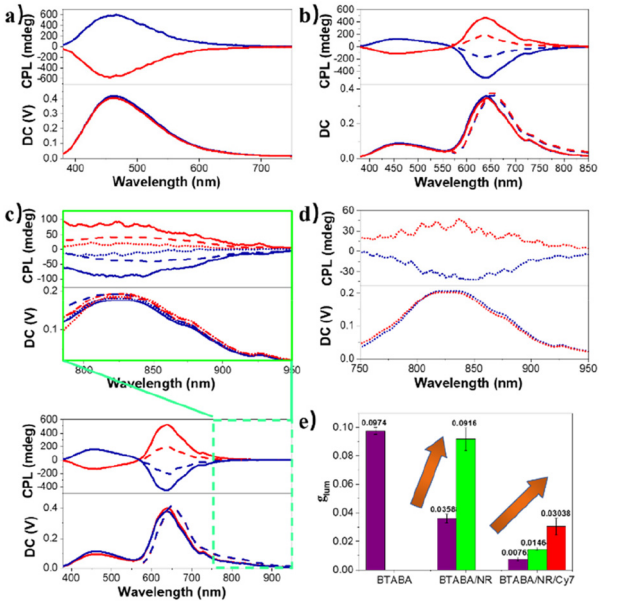

Fig. 4 (a) CPL spectra of the BTABA assembly. (b) Amplified CPL obtained after the energy transfer from donor BTABA to acceptor NR. (c) The BTABA/NR/CY7 assembly triad with cascade energy transfer showing stepwise amplified CPL. (d) CPL spectra of the BTABA/CY7 assembly. (e) Column diagrams of g_{lum} obtained by the irradiation of BTABA, NR or CY7. The CPL spectra belong to the samples of *M*-BTABA (blue line) and *P*-BTABA (red line). For the CPL spectra, the sample is excited at 330 nm (solid line), 532 nm (dashed line) or 730 nm (dotted line). [BTABA] = 5.29 mM, [NR] = 0.088 mM, [CY7] = 0.088 mM.

shown in Fig. 3a and b, the spiral structure of BTABA can induce achiral NR to adopt a twisted chiral conformation through non-covalent interactions. After that, we simulated the CD spectra of the BTABA/NR binary system and found that the CD signal of the acceptor is exactly opposite to the chiral signal of the BTABA assembly (Fig. 3f), which is in accordance with the experimental CD spectrum. This result suggests that the chiral conformation of BTABA molecules and the induced chiral NR have completely different angles between their magnetic and electric dipole moments.

We further investigated the chirality of excited states in this symmetry-breaking supramolecular system. Noteworthily, by applying the seeded-vortex strategy, controllably chiral BTABA assemblies were obtained, exhibiting a strong CPL signal at 465 nm with a g_{lum} value of approximately $\pm 9.74 \times 10^{-2}$ after 330 nm excitation (Fig. 4a). After BTABA co-assembling with NR, a new CPL peak at 647 nm appears that belongs to the chiral excited state of NR (Fig. 4b). If there are no chiral assemblies, then there is no CPL signal for the dye solution (Fig. S7†). Furthermore, upon the addition of the achiral dye CY7, a new peak belonging to CY7 appears at 825 nm (Fig. 4c). In the BTABA/CY7 co-assembly, although exciting BTABA fails to result in energy transfer to excite CY7, the directly exciting CY7 can generate 825 nm CPL with g_{lum} being equal to 5.6×10^{-3} (Fig. 4d and S8†). It suggests that BTABA cannot play the role of energy donor in BTABA/CY7, but it still works as a chiral host.

We further compared the CPL spectra of the acceptor by exciting the donor BTABA with CPL from the direct exciting acceptor. As shown in Fig. 4e and S8,† in the BTABA/NR assembly system, the g_{lum} value of the acceptor NR by exciting the donor BTABA (λ_{ex} = 330 nm) was 9.16×10^{-2}, which was 2.56 times larger than that obtained by directly exciting the NR acceptor (λ_{ex} = 532 nm). In the three-component assembly of BTABA/NR/CY7, a phenomenon of gradually amplified CPL through cascade energy transfer was observed. When the acceptor CY7 was directly excited at 730 nm, a weak CPL signal was obtained at 825 nm with a calculated g_{lum} value of 7.6×10^{-3}. When the intermediate acceptor NR was excited at 532 nm, CY7 emitted a significantly amplified CPL signal with a g_{lum} value of 1.46×10^{-2}. When the donor BTABA was excited at 330 nm, a strong CPL signal was obtained at 825 nm in the near-infrared region, and the g_{lum} value reached 3.04×10^{-2}, which was further enhanced compared to exciting the intermediate acceptor NR and was four times larger than excitation at 730 nm.[31,40]

As shown in Fig. 5a, we used a mobile telephone to directly detect emissions from all components in BTABA/NR/CY7, especially the near-infrared emission of CY7, which paved the way for output of multi-channel signals. In order to further understand the chiral assemblies, we used scanning electron microscopy (SEM) to characterize the morphology of all samples. As shown in Fig. 5b–e, BTABA has a good nanofiber

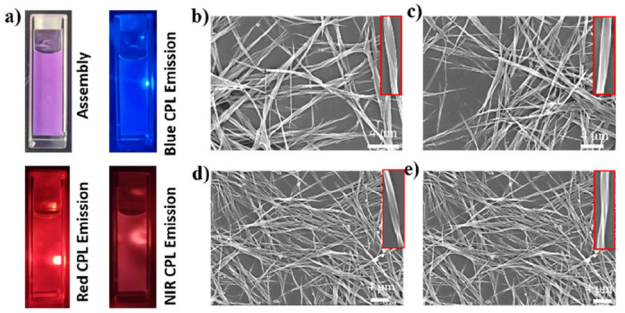

Fig. 5 (a) Photographs of BTABA/NR/CY7, which were captured using a mobile telephone assisted by filters to avoid other emissions. (b) SEM images of BTABA assemblies. (c) SEM images of BTABA/NR assemblies. (d) SEM images of BTABA/CY7 assemblies. (e) SEM images of BTABA/NR/CY7 assemblies. [BTABA] = 5.29 mM, [NR] = 0.088 mM, [CY7] = 0.088 mM.

structure. After incorporating the NR or CY7 acceptors, the nanostructure of the BTABA chiral assembly remained intact without obvious phase separation or aggregation. In addition, a series of regular diffraction peaks appeared in the XRD spectrum at 4.69°, 6.66°, 7.76°, 9.57°, 10.43° and 11.62° (Fig. S9a†), with distance ratios of approximately $1:\sqrt{2}:\sqrt{3}:\sqrt{4}:\sqrt{5}:\sqrt{6}$, indicating a layered stacking structure. As shown in Fig. S9b,† similar Fourier transform-infrared (FTIR) data were further used to analyse the interaction among dyes and BTABA molecules. The peak at 1664 cm^{-1} in the BTABA assembly is attributed to the characteristic peak of the carboxyl group in the BTABA assembly, indicating the formation of hydrogen bonds between the carboxylic acid groups of the adjacent molecules. The peak at 1600 cm^{-1} is attributed to the characteristic peak of the amide I band, and the peak at 1534 cm^{-1} is the amide II band. This proves the existence of hydrogen bonds between C═O and N–H. Thus, the FTIR result demonstrates that hydrogen bonds formed between molecules play a critical role in the assembly process. The FTIR spectra of BTABA/NR, BTABA/NR/CY7 and BTABA/CY7 show similar results, indicating that doping these non-chiral molecules does not destroy the tight molecular stacking of the BTABA assembly. The anisotropy of the BTABA sample was studied by polarized optical microscopy (POM) characteristics (Fig. S10†). BTABA, BTABA/NR, BTABA/NR/CY7 and BTABA/CY7 all showed nanofiber structures, indicating excellent stacking among the building blocks and dyes. This is consistent with the results of XRD and SEM.

Conclusions

In summary, we have successfully developed chiral nanofibers by combining supramolecular symmetry-breaking and fluorescence resonance energy transfer, resulting in the emergence of near-infrared circularly polarized luminescence with a high dissymmetry factor g_{lum}. Our approach involved harnessing the properties of achiral BTABA molecules to induce supramolecular chirality, which then co-assembled with achiral acceptors, NR and CY7. The BTABA/NR/CY7 system exhibited near-infrared CPL when excited by various wavelengths. Notably, a cascade energy transfer from BTABA to NR and subsequently to CY7 contributed to a substantial enhancement in the g_{lum} value of near-infrared CPL from CY7, reaching 0.03. This work introduces a novel strategy for creating materials with near-infrared CPL activity, even in exclusively achiral systems.

Conflicts of interest

There are no conflicts to declare.

Acknowledgements

This work was supported by the National Natural Science Foundation of China (51773021, 52173159 and 92256304).

Notes and references

1 H. U. Kim, T. Kim, C. Kim, M. Kim and T. Park, *Adv. Funct. Mater.*, 2023, **33**, 2208082.
2 Y. Gu, Z. Guo, W. Yuan, M. Kong, Y. Liu, Y. Liu, Y. Gao, W. Feng, F. Wang, J. Zhou, D. Jin and F. Li, *Nat. Photonics*, 2019, **13**, 525–531.
3 J. Liu, H. Liang, M. Li, Z. Luo, J. Zhang, X. Guo and K. Cai, *Biomaterials*, 2018, **157**, 107–124.
4 Kanika, G. Kedawat, S. Srivastava and B. K. Gupta, *Small*, 2023, 2206397.
5 F. Zinna and L. Di Bari, *Chirality*, 2015, **27**, 1–13.
6 J. P. Riehl and F. S. Richardson, *Chem. Rev.*, 1986, **86**, 1–16.
7 R. Amasaki, M. Kitahara, T. Kimoto, M. Fujiki and Y. Imai, *Eur. J. Inorg. Chem.*, 2022, e202101066.
8 T. Goto, Y. Okazaki, M. Ueki, Y. Kuwahara, M. Takafuji, R. Oda and H. Ihara, *Angew. Chem., Int. Ed.*, 2017, **56**, 2989–2993.
9 H. Oishi, S. Mashima, Y. Kuwahara, M. Takafuji, K. Yoshida, R. Oda, H. Qiu and H. Ihara, *J. Mater. Chem. C*, 2020, **8**, 8732–8735.
10 M.-M. Zhang, X.-Y. Dong, Z.-Y. Wang, X.-M. Luo, J.-H. Huang, S.-Q. Zang and T. C. W. Mak, *J. Am. Chem. Soc.*, 2021, **143**, 6048–6053.
11 N. F. M. Mukthar, N. D. Schley and G. Ung, *J. Am. Chem. Soc.*, 2022, **144**, 6148–6153.
12 B.-A. N. Willis, D. Schnable, N. D. Schley and G. Ung, *J. Am. Chem. Soc.*, 2022, **144**, 22421–22425.
13 J. Zhang, Q. Liu, W. Wu, J. Peng, H. Zhang, F. Song, B. He, X. Wang, H. H. Y. Sung, M. Chen, B. S. Li, S. H. Liu, J. W. Y. Lam and B. Z. Tang, *ACS Nano*, 2019, **13**, 3618–3628.
14 Y. Liu and P. Xing, *Adv. Mater.*, 2023, 2300968.
15 Q. Cheng, A. Hao and P. Xing, *ACS Nano*, 2022, **16**, 6825–6834.

16 G. Liu, L. Yao, K. Fu, S. Zheng, G. Yang and Y. Zhao, *Small Struct.*, 2022, **3**, 2200209.
17 B. Zhao, H. Yu, K. Pan, Z. Tan and J. Deng, *ACS Nano*, 2020, **14**, 3208–3218.
18 P. Xing and Y. Zhao, *Acc. Chem. Res.*, 2018, **51**, 2324–2334.
19 Y. Imai, Y. Nakano, T. Kawai and J. Yuasa, *Angew. Chem., Int. Ed.*, 2018, **57**, 8973–8978.
20 O. Oki, C. Kulkarni, H. Yamagishi, S. C. J. Meskers, Z.-H. Lin, J.-S. Huang, E. W. Meijer and Y. Yamamoto, *J. Am. Chem. Soc.*, 2021, **143**, 8772–8779.
21 L. Yao, K. Fu, X. Wang, M. He, W. Zhang, P.-Y. Liu, Y.-P. He and G. Liu, *ACS Nano*, 2023, **17**, 2159–2169.
22 Y. Shi, G. Yin, Z. Yan, P. Sang, M. Wang, R. Brzozowski, P. Eswara, L. Wojtas, Y. Zheng, X. Li and J. Cai, *J. Am. Chem. Soc.*, 2019, **141**, 12697–12706.
23 H. Zhang, X. Chang, C. Ma, G. Huang, B. S. Li and B. Z. Tang, *ACS Appl. Mater. Interfaces*, 2022, **14**, 43926–43936.
24 Z.-L. Gong, X. Zhu, Z. Zhou, S.-W. Zhang, D. Yang, B. Zhao, Y.-P. Zhang, J. Deng, Y. Cheng, Y.-X. Zheng, S.-Q. Zang, H. Kuang, P. Duan, M. Yuan, C.-F. Chen, Y. S. Zhao, Y.-W. Zhong, B. Z. Tang and M. Liu, *Sci. China: Chem.*, 2021, **64**, 2060–2104.
25 G. Zhou, P. Wang, B. Hu, X. Shen, C. Liu, W. Tao, P. Huang and L. Liu, *Nat. Commun.*, 2022, **13**, 4106.
26 F. Wang, F. Gan, C. Shen and H. Qiu, *J. Am. Chem. Soc.*, 2020, **142**, 16167–16172.
27 G. Zhou, T. Li, Y. Wu, P. Wang, K. Leng, C. Liu, Y. Shan and L. Liu, *Adv. Opt. Mater.*, 2020, **8**, 2000046.
28 J. M. Ribó, J. Crusats, F. Sagués, J. Claret and R. Rubires, *Science*, 2001, **292**, 2063–2066.
29 Y. Sang, D. Yang, P. Duan and M. Liu, *Chem. Sci.*, 2019, **10**, 2718–2724.
30 J. Wade, J. R. Brandt, D. Reger, F. Zinna, K. Y. Amsharov, N. Jux, D. L. Andrews and M. J. Fuchter, *Angew. Chem., Int. Ed.*, 2021, **60**, 222–227.
31 I. Z. Steinberg and B. Ehrenberg, *J. Chem. Phys.*, 1974, **61**, 3382–3386.
32 Z. Shen, T. Wang and M. Liu, *Angew. Chem., Int. Ed.*, 2014, **53**, 13424–13428.
33 M. M. J. Smulders, A. P. H. J. Schenning and E. W. Meijer, *J. Am. Chem. Soc.*, 2008, **130**, 606–611.
34 L. Stryer and R. P. Haugland, *Proc. Natl. Acad. Sci. U. S. A.*, 1967, **58**, 719–726.
35 J. Fan, M. Hu, P. Zhan and X. Peng, *Chem. Soc. Rev.*, 2013, **42**, 29–43.
36 A. Ajayaghosh, V. K. Praveen, C. Vijayakumar and S. J. George, *Angew. Chem., Int. Ed.*, 2007, **46**, 6260–6265.
37 C. Vijayakumar, V. K. Praveen and A. Ajayaghosh, *Adv. Mater.*, 2009, **21**, 2059–2063.
38 C. Vijayakumar, V. K. Praveen, K. K. Kartha and A. Ajayaghosh, *Phys. Chem. Chem. Phys.*, 2011, **13**, 4942–4949.
39 C. Du, X. Zhu, C. Yang and M. Liu, *Angew. Chem., Int. Ed.*, 2022, **61**, e202113979.
40 L. Ji, Y. Sang, G. Ouyang, D. Yang, P. Duan, Y. Jiang and M. Liu, *Angew. Chem., Int. Ed.*, 2019, **58**, 844–848.